SLAC–PUB–14534
September 2011

Femtosecond X-ray Pulse Temporal Characterization in Free-Electron Lasers Using a Transverse Deflector*

Y. Ding[1], C. Behrens[2], P. Emma[1], J. Frisch[1], Z. Huang[1],
H. Loos[1], P. Krejcik[1] and M-H. Wang[1]
[1] SLAC National Accelerator Laboratory, Menlo Park, CA 94025, USA
[2] Deutsches Elektronen-Synchrotron (DESY), Hamburg, Germany

Abstract

We propose a novel method to characterize the temporal duration and shape of femtosecond x-ray pulses in a free-electron laser (FEL) by measuring the time-resolved electron-beam energy loss and energy spread induced by the FEL process, with a transverse radio-frequency deflector located after the undulator. Its merits are simplicity, high resolution, wide diagnostic range, and non-invasive to user operation. When the system is applied to the Linac Coherent Light Source, the first hard x-ray free-electron laser in the world, it can provide single-shot measurements on the electron beam and x-ray pulses with a resolution on the order of 1-2 femtoseconds rms.

Submitted to the Phys. Rev. ST Accel. Beams.

*Work supported by Department of Energy contract DE–AC02–76SF00515.

I. INTRODUCTION

The successful operation of the Linac Coherent Light Source (LCLS) [1], with its capability of generating free-electron laser (FEL) x-ray pulses from a few femtoseconds (fs) up to a few hundred fs, opens up vast opportunities for studying atoms and molecules on this unprecedented ultrashort time scale. However, tremendous challenges remain in the measurement and control of these ultrashort pulses with femtosecond precision, for both the electron-beam (e-beam) and the x-ray pulses.

For ultrashort e-beam bunch length measurements, a standard method has been established at LCLS using an S-band radio-frequency (rf) deflector, which works like a streak camera for electrons and is capable of resolving bunch lengths as short as ~ 10 fs rms [1]. However, the e-beam with low charges of 20 pC at LCLS, which is expected to be less than 10 fs in duration, is too short to be measured using this transverse deflector [2]. Recently, a new method of measurement that maps time to energy has been demonstrated at LCLS, with a measured e-beam resolution about 1 fs rms [3].

The measurement of the electron bunch length is helpful in estimating the FEL x-ray pulse duration. However, for a realistic beam, such as that with a Gaussian shape or a spiky profile, the FEL amplification varies along the bunch due to peak current or emittance variation. This will cause differences between the temporal shape or duration of the electron bunch and the x-ray pulse. Initial experiments at LCLS have revealed that characterization of the x-ray pulse duration on a shot-by-shot basis is critical for the interpretation of the data. However, in the femtosecond regime, conventional photodetectors and streak cameras do not have a fast enough response time for characterizing the ultrashort x-ray pulses. Also, at the x-ray wavelengths, the vanishingly small cross-sections in nonlinear processes make temporal correlation techniques very challenging. To overcome these difficulties, some new methods have been studied recently. One of the time-domain methods is the terahertz-field-driven x-ray streak camera [4], where a terahertz field is used to modulate the photoelectrons generated from x-ray gas ionization. By measuring the energy distribution of the photoelectrons the x-ray pulse length can be determined. Here the terahertz radiation is generated from the same electron bunch in a dedicated undulator to achieve a synchronization between the x-ray and terahertz fields. An external laser has also been tested to streak the photoelectrons, but single-shot measurements are not possible due to synchronization difficulties [5].

In the frequency-domain, a statistical method is under study using multi-shot analysis of the spectral correlation function [6]. This technique has been experimentally demonstrated at LCLS, providing a multi-shot based x-ray pulse duration measurement. There are also other techniques proposed or tested, such as x-ray auto-correlation or x-ray gas interactions [7, 8].

We propose a novel method in this paper to characterize the FEL x-ray pulse duration and shape. A transverse rf deflector is used in conjunction with an e-beam energy spectrometer, located after the FEL undulator. By measuring the difference in the e-beam longitudinal phase space between FEL-on and FEL-off, we can obtain the time-resolved energy loss and energy spread induced from the FEL radiation, allowing the FEL x-ray temporal shape to be reconstructed. This is a simple, single shot method that is non-invasive to the FEL operation. The X-band transverse deflector that has been designed for the LCLS will cover the diagnostic range from a few fs to a few hundred fs over the full range of the FEL radiation wavelengths.

II. RF DEFLECTOR AND SYSTEM LAYOUT

The idea of using an rf deflecting structure (operating in the TM11 mode) to kick the electron beam was first proposed in 1960s [9], and has been recently used for e-beam bunch length measurements in FELs and other accelerator facilities [10]. We assume the bunch is deflected in horizontal plane by the high-frequency time-variation of the deflecting fields, where the resulting horizontal beam width measured on a downstream screen (with a phase advance near $\pi/2$) represents a single-shot measure of the absolute bunch length. This horizontally "streaked" e-beam is then sent to an energy spectrometer, which is composed of dipoles and quadrupoles providing large vertical momentum dispersion. If the optics is designed to have a vertical beta function small enough at the downstream screen, the vertical beam extent across the screen represents a momentum spread in the beam. With this setup the e-beam longitudinal phase space (time and energy) is mapped into the transverse dimensions (horizontal and vertical).

In the FEL process, the interaction between an e-beam and an electromagnetic wave leads to e-beam energy modulation at the fundamental radiation wavelength. As electrons wiggling in the undulator, a periodic density modulation (the so-called "microbunching") at

the radiation wavelength builds up. The microbunched e-beam then emits coherent radiation at the expense of the electron kinetic energy. The collective interaction of the beam-radiation system leads to an exponential growth of the radiation intensity along the undulator distance. As a result, it causes electron energy loss and energy spread increase and FEL power reaches saturation. At LCLS, the typical FEL-induced electron energy loss at saturation is more than 10 MeV [1]. To obtain the x-ray temporal profile, we first suppress the FEL process (e.g., by kicking e-beam to make a local oscillating orbit inside the undulator) and measure the e-beam time-energy phase space, from which we can get the e-beam temporal profile and also achieve a baseline on the energy loss. Next, the FEL is restored and measure the time-energy phase space again for each bunch. By subtracting the baseline measured with FEL-off, we can obtain the time-resolved energy loss or energy spread due to FEL radiation, shot by shot. The x-ray temporal power profile is then determined by combining the e-beam current profile and the time-resolved energy loss.

Figure 1 shows the beamline layout of the diagnostic system to be installed at the end of the LCLS main undulator. We use two 1-meter long X-band rf deflecting structures to provide a maximum of 46 MeV/c horizontal kick, with 40 MW input rf power at the deflecting structure [11].

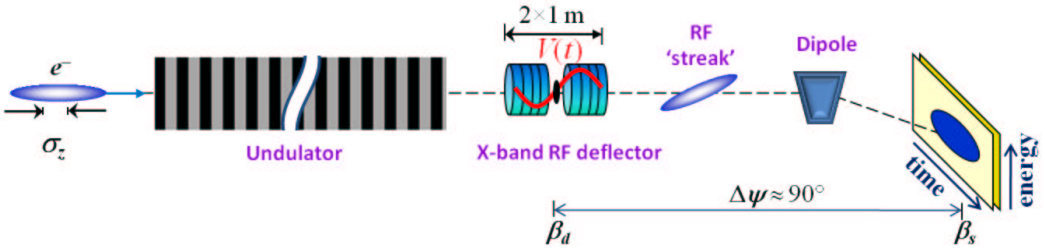

FIG. 1: A layout of the diagnostic system with a transverse rf deflector and an energy spectrometer.

III. APPLICATION OF THE METHOD

The deflecting force imparts a transverse momentum on the bunch with a small kick angle, $\Delta x\prime$, given by

$$\Delta x\prime(t) = \frac{eV_0}{pc}\sin(2\pi ct/\lambda + \varphi) \approx \frac{eV_0}{pc}(\frac{2\pi}{\lambda}ct\cos\varphi + \sin\varphi), \quad (1)$$

where V_0 is the deflector peak voltage, p is the beam's longitudinal momentum in the structure, $\lambda = 2.63$ cm is the rf wavelength, φ is the rf phase (=0 at zero-crossing), and t is the electron time coordinate relative to the bunch center. The approximation is made that the bunch length much shorter than the rf wavelength, $|ct| \ll \lambda/2\pi$.

From the deflecting point to the downstream screen, the beam is transported through a transfer matrix with angular-to-spatial element $R_{12} = (\beta_{xd}\beta_{xs})^{1/2}\sin\Delta\Psi$. Here β_{xd} and β_{xs} are the horizontal beta functions at the deflector and the screen, respectively, and $\Delta\Psi$ is the horizontal betatron phase advance from deflector to screen. The transverse position of each ultra-relativistic electron on the screen is then given

$$\Delta x(t) = \frac{eV_0}{pc}\sqrt{\beta_{xd}\beta_{xs}}|\sin\Delta\Psi|(\frac{2\pi}{\lambda}ct\cos\varphi + \sin\varphi). \tag{2}$$

From Eq. (2) it is clear that for bunch length measurement, operating at the zero-crossing phase ($\varphi = 0$) gives the best streaking effects with the horizontal beam size corresponding to bunch length ($\sigma_x \propto c\sigma_t$), while $\sin\varphi \neq 0$ gives a centroid offset which can be used for calibration ($\langle\Delta x\rangle \propto \sin\varphi$). For example, by measuring the horizontal centroid offset with a small rf phase shift around zero-crossing, the size of horizontal dimension is calibrated relative to the absolute rf wavelength. From Eq. (2), near zero-crossing, the time calibration factor can be written as

$$S = \frac{\sigma_x}{c\sigma_t} = \frac{eV_0}{pc}\sqrt{\beta_{xd}\beta_{xs}}|\sin\Delta\Psi|\frac{2\pi}{\lambda}. \tag{3}$$

For the LCLS e-beam high-energy case of 14 GeV, based on the parameters listed in Table I, $S = 128$. This means if the measured horizontal beam size $\sigma_x = 128\mu$m, the actual bunch length is $c\sigma_t = 1\mu$m.

Note that an X-band rf deflector has been chosen over S-band like the original transverse deflector [9] in order to impart a stronger sweep to the beam and improve the temporal resolution. At X-band the rf wavelength, λ, is smaller, giving a factor 4 improvement in Eq. (2). Furthermore, higher rf gradients can be achieved at X-band, allowing V_0 to be increased and further improving the gain in Eq. (2).

The vertical beam size measured after the vertically-bent spectrometer represents the electron energy deviation, which is given by

$$\Delta y = \eta_y\delta, \tag{4}$$

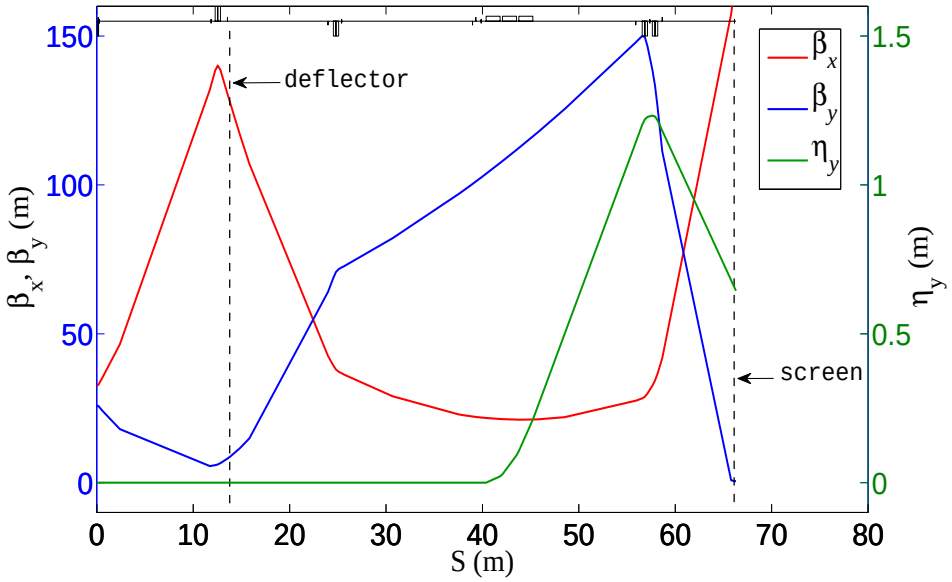

FIG. 2: The optics layout for this diagnostics. The locations of the deflector and screen are marked in the picture.

where η_y is the vertical momentum dispersion function at the screen, and δ is the relative energy deviation before the energy spectrometer. Note now we have a two-dimensional image with x representing to time, and y representing to energy.

As seen from Eq. (2) and (4), the beam transportation optics should be optimized to achieve the best resolution. Larger horizontal beta function at deflector and smaller vertical beta function at screen are preferred. The optics beta and dispersion functions for the high-energy (14 GeV) case are shown in Fig. 2 for the existing LCLS beamline magnets after their strengths have been adjusted to optimize the beta functions. In this example, the horizontal $\beta_{xd} = 120$ m, $\beta_{xs} = 170$ m, the phase advance $\Delta\Psi = 90°$, the vertical beta function at the screen $\beta_{ys} = 0.54$ m, and the dispersive function $\eta_y = 0.65$ m. A very similar optics setup has also been achieved at low electron-energy (4.3 GeV) for soft x-ray generation.

Temporal resolution $\sigma_{t,r}$ and energy resolution $\sigma_{E,r}$ can be defined as

$$\sigma_{t,r} = \frac{\sigma_{x0}}{cS}, \quad \sigma_{E,r} = \frac{\sigma_{y0}}{\eta_y} E_0, \tag{5}$$

where σ_{x0} or σ_{y0} is the nominal transverse beam size at the screen (i.e., in the absence of deflecting voltage for σ_{x0}, and in the absence of dispersion for σ_{y0}), and E_0 is the average electron energy.

The main parameters are summarized in Table I, based on a normalized projected-emittance of 0.6μm. The potential temporal resolution is $\sim$1 fs rms for LCLS soft x-rays, and $\sim$ 2 fs for hard x-rays.

TABLE I: X-band transverse deflector parameters.

Parameter	**Symbol**	**Value**	**Unit**
RFr frequency	f	11.424	GHz
Deflecting structure length	L	2×1	m
RF input power	P	40	MW
Deflecting voltage (on crest)	V_0	48	MV
Soft x-ray (e-beam 4.3 GeV)			
Calibration factor	S	400	
Temporal resolution (rms)	$\sigma_{t,r}$	$\sim$1	fs
Energy resolution (rms)	$\sigma_{E,r}$	56	keV
Hard x-ray (e-beam 14 GeV)			
Calibration factor	S	128	
Temporal resolution (rms)	$\sigma_{t,r}$	$\sim$2	fs
Energy resolution (rms)	$\sigma_{E,r}$	100	keV

IV. SIMULATION STUDIES

Start-to-end simulations have been carried out to verify this scheme. IMPACT-T [12] and ELEGANT [13] codes have been used in the injector and main linac, including bunch compressors. In the undulator, a 3-dimensional (3D) FEL simulation code GENESIS [14] has been adopted for FEL simulations, where the resistive wake fields from undulator chamber and the spontaneous undulator radiation are also included. At the end of the undulator, the dumped particles are used again by ELEGANT to track them through the transverse deflector and energy spectrometer down to the dump screen. From the simulated images at the dump screen, we can analyze the x-ray pulse duration.

We first show an example of the LCLS hard x-ray case (radiation wavelength of 1.5 Å, e-beam energy of 13.6 GeV, total undulator length of 132m including breaks) with a nominal

operating charge of 250 pC. The average e-beam peak current is about 3 kA. Since the resistive wake fields in the linac rf structure introduce a third-order nonlinear curvature in the longitudinal phase space, we typically have a "double-horn" shape in the current profile. It is of great importance and interest to characterize the lasing process from this complicated bunch shape.

Figure 3(a) and 3(b) shows the simulated "measurements" of the projected transverse images at the dump screen, with the horizontal axis representing time, and the vertical axis representing energy. Clearly, we can see the difference in the energy dimension between FEL-on and FEL-off. From the case of FEL-off (Fig. 3(a)), we get the time-resolved e-beam energy ($E_{FELoff}(t)$) and energy spread ($\sigma_{E_{FELoff}}(t)$). The major collective effects include those from undulator chamber wakes, undulator spontaneous radiation, transverse deflecting effect and coherent synchrotron radiation (CSR) in spectrometer dipoles. When switched on, the FEL radiation introduces an additional energy loss ($\Delta E_{FEL}(t)$) and energy spread ($\sigma_{E_{FEL}}(t)$). We obtain the e-beam energy (E_{FELon}) and energy spread ($\sigma_{E_{FELon}}$) for the FEL-on case from Fig. 3(b). From the two measurements we can determine the time-sliced energy loss or energy spread increase purely induced from FEL radiation:

$$\begin{aligned} \Delta E_{FEL}(t) &= E_{FELoff}(t) - E_{FELon}(t), \\ \sigma_{E_{FEL}}(t) &= \sqrt{\sigma^2_{E_{FELon}}(t) - \sigma^2_{E_{FELoff}}(t)}. \end{aligned} \tag{6}$$

The horizontal projection of the images in Fig. 3(a) and 3(b) represents the e-beam temporal profile. The transverse deflector method provides an additional technique for eliminating systematic correlation errors. The upstream bunch compressors in the LCLS are in the horizontal plane and the CSR from their bends introduces a transverse kick to the electrons which is correlated to their longitudinal position in the bunch [15]. This correlation between the horizontal and longitudinal planes can affect the phase space reconstruction technique because the deflector also streaks the beam horizontally. This effect can be canceled by performing a second measurement at the other rf zero-crossing phase, 180° from the first measurement [16]. An effective calibration factor is defined after the dual rf zero-crossing measurements. Figure 3(c) shows the reconstructed e-beam current profile from two zero-crossing phases comparing the original one.

With the obtained time-sliced energy loss and current, the x-ray power profile is directly

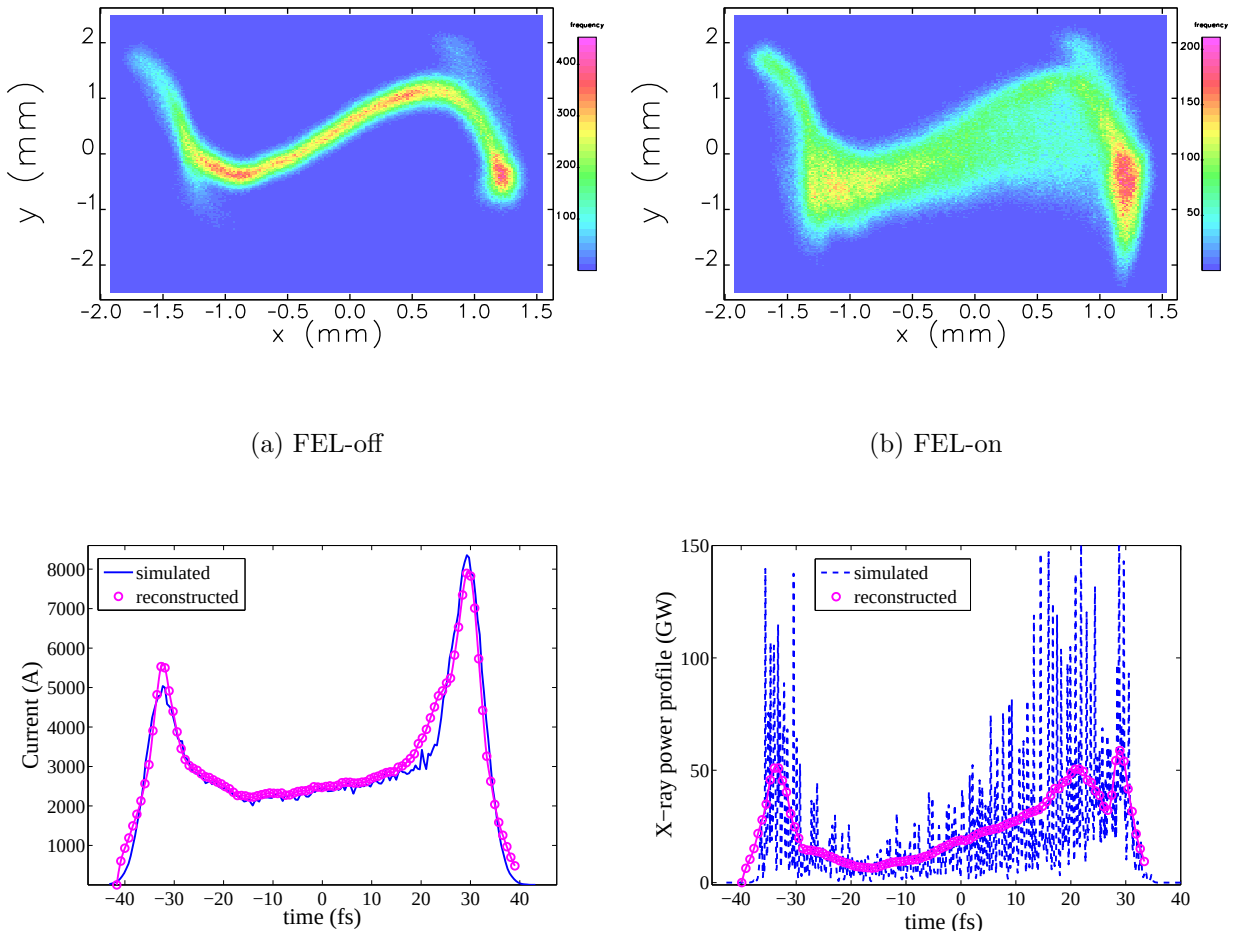

(a) FEL-off

(b) FEL-on

(c) e-beam current profile

(d) x-ray profile

FIG. 3: The simulated images on the screen representing e-beam longitudinal phase space for FEL-off (a) and FEL-on (b). The bunch charge is 250 pC with an energy of 13.6 GeV. (c) and (d) show the reconstructed e-beam current and FEL x-ray profiles comparing with the simulated ones. Bunch head is to the left.

determined with an absolute power scale ($P(t) = \Delta E_{FEL}(t) \times I(t)$). The reconstructed x-ray profile from the energy loss for this hard x-ray example is shown in Fig. 3(d). Since LCLS is operating in the self-amplified spontaneous emission (SASE) mode, there are many longitudinal spikes whose typical width is ∼0.2 fs in this hard x-ray wavelength. The reconstructed pulse shape is a smooth approximation to the actual profile, where the finer spikes are smeared out by the limited temporal resolution. Using the energy spread data we get

a similar x-ray profile. To obtain the absolute power scale from the energy spread analysis requires an additional measurement of the total x-ray pulse energy.

Comparing the e-beam current profile and the x-ray profile shown in Fig. 3, we can see that the shape of the x-ray profile deviates from the e-beam current profile, with less lasing right after the horn at the head of the bunch. This is the result of wakefields in the undulator chamber from the horn at the head of the bunch suppressing the FEL lasing.

Low charge operation mode with 20 pC at LCLS has been used in many x-ray user experiments to produce x-ray pulses of a few fs duration [2]. Since these short x-ray pulses typically only have a few spikes, there is a large variation on the pulse shape. This makes the measurement of the actual x-ray pulse profile even more critical. We show an example of the soft x-ray case right after saturation. The bunch charge is 20 pC and energy is at 4.3 GeV. In the second bunch compressor the e-beam is over-compressed so we can have a Gaussian-like current profile to generate a shorter x-ray pulse [2]. The longitudinal phase space simulated at the dump screen is shown in Fig. 4. Compare the two images with FEL-on and FEL-off, we obtained the x-ray profile (Fig. 4(d)). The e-beam is about 4 fs FWHM, and the FEL profile in this snapshot has one main spike, and two small side spikes. Comparing the reconstructed profiles with the simulated ones, we see some distortions in the profile peaks but still it is very encouraging. Running into the deep saturation regime, the slippage effect between FEL and e-beam may affect the shape of the reconstructed x-ray power profile, especially for long-wavelength radiations. In the x-ray wavelengths, this slippage effect after saturation is not a problem.

V. DISCUSSIONS AND SUMMARY

As described earlier, we suppress FEL lasing process and record the e-beam longitudinal phase space as a baseline, then compare the FEL-on case with the saved baseline image to analyze the FEL x-ray profile. The pulse-by-pulse jitter issues have to be considered during the measurements. By choosing the X-band rf deflector, an increased temporal resolution has been achieved, but the price to be paid is an increased sensitivity to phase jitter between the bunch arrival time and the X-band rf system. This must be minimized by designing tight rf phase tolerances into the system. The present achievable X-band rf phase stability could be $< 0.1^{\circ}$, however, the measured LCLS arrival time jitter is $\sim$50 fs rms [1]. This beam arrival

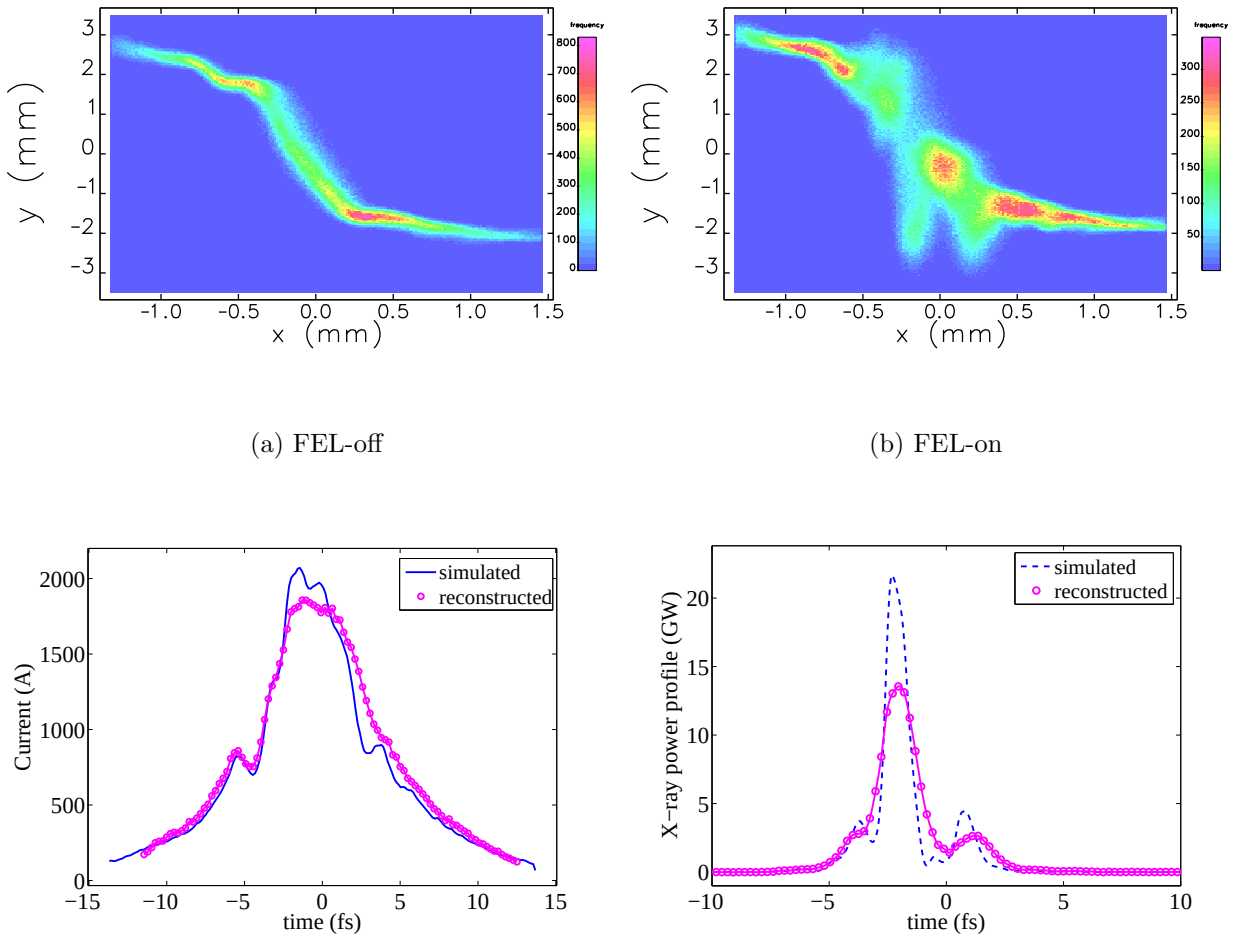

(a) FEL-off

(b) FEL-on

(c) e-beam current profile

(d) x-ray profile

FIG. 4: The simulated images on the screen representing e-beam longitudinal phase space for FEL-off (a) and FEL-on (b). The bunch charge is 20 pC with an energy of 4.3 GeV. (c) and (d) show the reconstructed e-beam current and FEL x-ray profiles comparing with the simulated ones. Bunch head is to the left.

time jitter makes the calibration very difficult. At LCLS, two phase cavities located after the undulator are used to measure the beam arrival time with an accuracy of ∼10 fs rms [17]. These arrival time data measured from the phase cavities can be used to correct the timing jitter during the transverse deflector calibration measurements. With this correction we can achieve a pretty good calibration within a reasonable rf phase range based on multishots average. Since we operate at the zero-crossing phase region which is quite linear, these rf phase jitter and beam arrival jitter does not affect the phase space measurement, though

a relatively large screen should be considered for the system design. The e-beam pulse-by-pulse energy jitter can also be corrected with the beam position monitors (BPMs) in the dogleg before the undulator. The transverse jitter out of the undulator is small and does not cause additional effect on the measurement.

In summary, we have shown that the proposed transverse rf deflector located after the FEL undulator has the potential to reconstruct the x-ray temporal profiles by measuring the e-beam longitudinal phase space with a very high resolution down to a few fs. This single-shot method is widely applicable to any radiation wavelength, SASE or seeded FEL mode, without interruption to user operation. This data can be delivered to the x-ray experiments in real time on a pulse by pulse basis. In addition, the e-beam bunch length is also obtained, proving a useful tool for a detailed study on the FEL lasing process.

We thank G. Bowden, V. Dolgashev, J. Wang, J. Welch and D. Xiang for helpful discussions. This work was supported by Department of Energy Contract No. DE-AC02-76SF00515.

---

[1] P. Emma *et al.*, Nat. Photon. **4**, 641 (2010).

[2] Y. Ding *et al.*, Phys. Rev. Lett. **102**, 254801 (2009).

[3] Z. Huang *et al.*, Phys. Rev. ST Accel. Beams **13**, 092801 (2010); Z. Huang *et al.*, PAC11.

[4] U. Frühling *et al.*, Nat. Photon. **3**, 523 (2009).

[5] A. Maier, private discussion.

[6] A. Lutman *et al.*, submitted to PRL

[7] G. Geloni *et al.*, DESY 10-008, arXiv:1001.3544v1.

[8] S. Dusterer *et al.*, submitted to New Journal of Physics.

[9] G. A. Loew, O. H. Altenmueller, Design and applications of R.F. deflecting structures at SLAC, SLAC-PUB-135, Aug. 1965.

[10] For example, see R. Akre *et al.*, EPAC 2002, p1882; Z. Huang *et al.*, Phys. Rev. ST Accel. Beams **13**, 020703 (2010); M. Röhrs *et al.*, Phys. Rev. ST Accel. Beams **12**, 050704 (2009);P. Musumeci *et al.*, Phys. Rev. Lett., **106**, 184801 (2011).

[11] J. Wang and S. Tantawi, Proceedings of LINAC 08, Victoria, BC, Canada.

[12] J. Qiang *et al.*, Phys. Rev. ST Accel. Beams **9**, 044204 (2006).

[13] M. Borland, *Elegant*, Advanced Photon Source LS-287, 2000.

[14] S. Reiche *et al.*, Nucl. Instrum. Methods Phys. Res. Sect. A **429**, 243 (1999).

[15] K. Bane *et. al.*, Phys. Rev. ST Accel. Beams **12**, 030704 (2009).

[16] H. Loos *et al.*, Proceedings of FEL2005, p632, Stanford, CA (2005).

[17] A. Brachmann *et al.*, IPAC10; see also SLAC-PUB-14234.